Ferromagnetism and nonlocal correlations in the Hubbard model

S. Henning* and W. Nolting

Lehrstuhl Festkörpertheorie, Institut für Physik, Humboldt-Universität zu Berlin, Newtonstrasse 15, 12489 Berlin, Germany

(Received 4 January 2012; published 16 March 2012)

We study the possibility and stability of band ferromagnetism in the single-band Hubbard model for the simple cubic (sc) lattice. A nonlocal self-energy is derived within a modified perturbation theory. Results for the spectral density and quasiparticle density of states are shown with special attention to the effects of **k** dependence. The importance of nonlocal correlations for the fulfillment of the Mermin-Wagner theorem is our main result. A phase diagram showing regions of ferromagnetic order is calculated for the three-dimensional lattice. Besides, we show results for the optical conductivity and prove that the renormalized one-loop contribution to the conductivity already cancels the Drude peak exactly in case of a local self-energy which is not true anymore for a nonlocal self-energy.

DOI: 10.1103/PhysRevB.85.125114 PACS number(s): 71.10.Fd, 75.10.Jm, 75.10.Lp

I. INTRODUCTION

Band ferromagnetism is bound to the existence of permanent magnetic moments belonging to itinerant electrons in a partially filled conduction band.[1] Archetypical representatives are the classical 3*d* ferromagnets Fe, Co, Ni. The microscopic interpretation of band ferromagnetism is one of the most fundamental and also most complicated many-particle problems in condensed matter physics. It is expected to be due to the interplay between ordinary, spin-independent Coulomb interaction (strong and strongly screened) and kinetic energy in the frame determined by the Pauli principle.

A minimal model for the investigation of band ferromagnetism was proposed independently by Hubbard,[2] Kanamori,[3] and Gutzwiller.[4] Despite its simple appearance, the Hubbard model Hamiltonian forms a highly nontrivial many body problem that cannot be treated rigorously for the general case.

A big step forward in the understanding of correlation effects in the Hubbard model was the invention of the *dynamical mean field theory* (DMFT), which becomes an exact theory in the limit of infinite lattice dimensions.[5–7] The DMFT maps the lattice problem onto an effective single-impurity Anderson model (SIAM) which can be solved numerically, essentially exactly by use of, for example, quantum Monte Carlo methods.[8]

One shortcoming of the otherwise highly successful DMFT is the locality (wave-vector independence) of the electronic self-energy strictly valid only for $d = \infty$. So it may be questionable, for example, whether such a self-energy is sufficient to describe angle-resolved photoemission results. Recent efforts have therefore been focused on regaining a certain degree of nonlocality in the DMFT self-energy.[9–13]

There are other approaches to the nonlocality of the self-energy at low dimensions $d = 2,3$. Coming from the weak coupling limit, Schweitzer and Czycholl proposed a method for solving the highly involved wave vector summations that already appear in second-order diagrammatic perturbation theory.[14] Kakehashi and Fulde used a projection operator method combined with the coherent potential approximation for an investigation of the nonlocal excitation spectra.[15]

Concerning ferromagnetism, the few exactly known results for the Hubbard model are of great value and can be used as a test frame for approximate theories. The Nagaoka theorem[16] states that a saturated ferromagnetic order is the ground state for $U = \infty$ when one hole/electron is introduced into the half-filled band for the simple cubic (sc) lattice in three dimensions (3D). The Mermin-Wagner theorem[17] rules out ferromagnetic and antiferromagnetic order in the Hubbard model in dimensions $d \leqslant 2$ for finite temperatures.[18–20] For the infinite dimensional sc and fcc lattice the existence of ferromagnetism was proved by DMFT calculations.[21–24]

Apart from these rigorous results, several works have investigated the possibility of ferromagnetism in the Hubbard model within an approximation. DMFT calculations were done for the 3D sc and fcc lattice[23,25] and the influence of next-nearest-neighbor hopping was investigated in Ref. 26. Ferromagnetism in various lattices was investigated with a spectral density approach (SDA) self-energy in Refs. 27 and 28. Variational methods have been used in Refs. 29–31.

A general trend can be read from these calculations. Two main ingredients favor ferromagnetism in the Hubbard model. An asymmetric density of states (DOS) (e.g., the fcc DOS) and nonbipartite lattices with frustration in the antiferromagnetic correlations, which can be generated by introducing next-nearest-neighbor hopping t'. This shows the competitive character of ferro- and antiferromagnetic correlations in the Hubbard model.

In this paper we investigate the influence of nonlocal correlations on ferromagnetic order in the sc lattice. To this end we shall apply the *modified perturbation theory* (MPT), which was originally used only for solving the SIAM within the DMFT procedure, directly to the full Hubbard problem. The MPT leads to an explicitly wave-vector dependent self-energy which decisively determines the single-electron spectral density. It is well known that the latter provides the bare line shape of a spin and angle-resolved (direct or inverse) photoemission experiment.

The paper is organized as follows. In Sec. II we introduce the Hubbard model Hamiltonian, derive the MPT self-energy, and discuss its properties. Then thermodynamic quantities as the paramagnetic static susceptibility and the optical conductivity are derived. In Sec. III the numerical methods for dealing with the complicated momentum summations are presented. Section IV contains the results and interpretation of our numerical calculations. Finally we give a summary and conclusion in Sec. V.

II. THEORY

A. Hubbard model

The Hamiltonian of the Hubbard model is given by

$$H = t \sum_{\langle i,j\rangle\sigma} c^{+}_{i\sigma} c_{j\sigma} + \sum_{i\sigma} (z_\sigma B + t_0)\hat{n}_{i\sigma} + U \sum_i \hat{n}_{i,\uparrow}\hat{n}_{i,\downarrow}. \quad (1)$$

Here t denotes the nearest-neighbor hopping strength (the sum over $\mathbf{R}_j$ extends only over the nearest neighbors of $\mathbf{R}_i$), U is the local Coulomb repulsion, and B is an homogeneous external magnetic field ($z_{\uparrow\downarrow} = \pm 1$). We have chosen the band center of gravity $t_0 = 0$ and the hopping strength t such that the free electronic bandwidth W is equal to one throughout the paper. An (approximate) solution of the Hubbard model is found if we are able to calculate the electronic Green's function (GF):

$$G_{\mathbf{k}\sigma}(E) = [E + \mu - \epsilon(\mathbf{k}) - \Sigma_{\mathbf{k}\sigma}(E)]^{-1} \quad (2)$$

or more precisely the electronic self-energy $\Sigma_{\mathbf{k}\sigma}(E)$.

B. Self-energy

It is now a well-known fact that the self-energy of the Hubbard model becomes a purely local quantity in the limit of infinite dimensions ($d \to \infty$).[5,6] However the $\mathbf{k}$ dependence will certainly play a crucial role in the more realistic case of $d = 2,3$. In the weak coupling limit ($U \ll W$) the second-order perturbation theory (SOPT) is a good starting point for the investigation of nonlocal correlation effects. The SOPT self-energy is given by[14]

$$\begin{aligned}\Sigma_{\mathbf{k}\sigma}(E) &= \Sigma^{(\mathrm{HF})}_{\sigma} + \Sigma^{(\mathrm{SOC})}_{\mathbf{k}\sigma}(E) \\ &= U\langle n_{-\sigma}\rangle + U^2 \sum_{\mathbf{R}} e^{i\mathbf{k}\mathbf{R}} \int dx S_{\mathbf{R}\sigma}(x) \int dy S_{\mathbf{R}-\sigma}(y) \int dz S_{-\mathbf{R}-\sigma}(z) \frac{f_-(x)f_-(y)f_-(-z) + f_-(-x)f_-(-y)f_-(z)}{E + i0^+ - x - y + z}. \quad (3)\end{aligned}$$

The sum extends over all lattice sites $\mathbf{R}$. Schweitzer and Czycholl[14] gave a method for the calculation of (3) by collecting all symmetry equivalent points in shells and recast the sum over lattice sites into a sum over shells. They showed that this sum can be truncated after a finite number of shells. However, their method of calculating the real and imaginary part of (3) is still numerically very demanding. We will show in Sec. III how to speed up the computation to allow fully self-consistent calculations for arbitrary band fillings n. There is a certain arbitrariness in (3) concerning the spectral densities (SD) appearing in the formula. In an expansion strictly to order U^2 the free SD has to be chosen.[32] But one could also renormalize the theory by using the full SD in a self-consistent manner. It turns out that only the first choice will reproduce certain exact results.[33] To be specific we give the form of the SD used:

$$S^{(0)}_{\mathbf{R}\sigma}(x) = \frac{1}{N} \sum_{\mathbf{k}} e^{i\mathbf{k}\mathbf{R}} \delta\left[x + \mu^{(0)}_{\sigma} - \epsilon(\mathbf{k})\right]. \quad (4)$$

$\mu^{(0)}_{\sigma}$ is fixed by the condition that the free occupation number is equal to the full occupation: $\langle n_\sigma\rangle^{(0)} = \langle n_\sigma\rangle$. Notice that this choice of $\mu^{(0)}_{\sigma}$ is equivalent to a SOPT "around Hartree-Fock (HF)" at half-filling where the full μ from (2) is taken in the HF-SD. Only this choice will result in the now widely accepted three peak structure of the density of states (DOS) and will give a "smooth" change of the DOS away from half-filling. For more qualitative discussions we refer the reader to the Results section.

To extend the validity of the self-energy to larger values of U we use the following ansatz for a modified perturbation theory (MPT):

$$\Sigma_{\mathbf{k}\sigma}(E) = U\langle n_{-\sigma}\rangle + \frac{a_{\mathbf{k}\sigma}\,\Sigma^{(\mathrm{SOC})}_{\mathbf{k}\sigma}(E)}{1 - b_{\mathbf{k}\sigma}\,\Sigma^{(\mathrm{SOC})}_{\mathbf{k}\sigma}(E)}. \quad (5)$$

This form for the self-energy was proposed by Kajueter and Kotliar[34] for the Anderson impurity model (SIAM). They used the first two spectral moments and an additional condition for the chemical potential to fix the parameters $a_{\mathbf{k}\sigma}$ and $b_{\mathbf{k}\sigma}$. This method of fixing the parameters was afterwards modified by Potthoff *et al.*[35] for the same model in order to reproduce the first four moments of the SD correctly. We will follow this latter approach but now applied to the full lattice Hamiltonian (1).

To fix the appearing constants in (5) we use the high-energy expansion of the self-energy for the Hubbard model:

$$\Sigma_{\mathbf{k}\sigma}(E) = \sum_{m=0}^{\infty} \frac{C^{(m)}_{\mathbf{k}\sigma}}{E^m}. \quad (6)$$

The first three coefficients can be obtained from the first four moments $M^{(m)}_{\mathbf{k}\sigma}$ of the SD[20] via the high-energy expansion of the electronic GF (2):

$$G_{\mathbf{k}\sigma}(E) = \frac{1}{E} \sum_{m=0}^{\infty} \frac{M^{(m)}_{\mathbf{k}\sigma}}{E^m} \quad (7)$$

and are given in (A1). By expanding also the right-hand side of (5) we can determine the coefficients $a_{\mathbf{k}\sigma}, b_{\mathbf{k}\sigma}$ and get finally the MPT self-energy:

$$\Sigma_{\mathbf{k}\sigma}(E) = U\langle n_{-\sigma}\rangle + \left\{ \left[\Sigma^{(\mathrm{SOC})}_{\mathbf{k}\sigma}(E)\right]^{-1} + \frac{D^{(2)}_{\mathbf{k}\sigma} - C^{(2)}_{\mathbf{k}\sigma}}{\left(C^{(1)}_{\mathbf{k}\sigma}\right)^2} \right\}^{-1}, \quad (8)$$

where $D^{(2)}_{\mathbf{k}\sigma}$ denotes the third moment of (3) as given in (B2).

The MPT self-energy can be proved to be exact in a variety of limiting cases. It trivially fulfills the limits of $U = 0$ and

$n = 0, n = 2$. More interesting is the case of zero bandwidth limit $t \to 0$. A straightforward calculation yields

$$\Sigma_{\mathbf{k}\sigma}^{(W\to 0)}(E) = U\langle n_{-\sigma}\rangle + \frac{U^2\langle n_{-\sigma}\rangle(1-\langle n_{-\sigma}\rangle)}{E + z_\sigma B + \mu - U(1-\langle n_{-\sigma}\rangle)}, \tag{9}$$

which is indeed the correct form of the "atomic limit."[20] Expanding the self-energy for small U reproduces the result of perturbation theory (3) with corrections only of order U^3. Therefore the MPT should be correct for small U and show, for example, Fermi liquid behavior.[14]

Since the first four spectral moments are reproduced correctly by construction, they should be correct at large energies $|E| \gg 1$, too. In particular, the position and shape of the upper (lower) Hubbard band for $n < 1$ ($n > 1$) will become exact in the strong coupling limit ($U \gg 1$) which is known to be a weak point of SOPT alone. In this respect the MPT self-energy is in accordance with the t/U strong coupling expansion of Harris and Lange.[36,37] To conclude this discussion we summarize our findings. We have proposed a fully **k**-dependent MPT self-energy which fulfills the atomic limit and shows reasonable behavior in the weak and strong coupling region. Therefore there is well-founded hope that our theory will also give reasonable results in the intermediate coupling region.

C. Thermodynamics and transport

1. Paramagnetic static susceptibility

The developed theory allows for a self-consistent calculation of the magnetization in a possible appearing ferromagnetic region. To test the system regarding a ferromagnetic phase transition, we will calculate the paramagnetic static susceptibility, which is defined as follows:

$$\hat{\chi}^{(p)}(T) = \sum_\sigma \partial_B(z_\sigma\langle n_\sigma\rangle)|_{T,B=0,\langle n_\uparrow\rangle=\langle n_\downarrow\rangle}. \tag{10}$$

The zero crossings of the inverse of (10) indicate the points where the paramagnetic phase become susceptible to a ferromagnetic phase transition.

For an evaluation of (10) one has to perform the derivative analytically and get after a lengthy calculation an explicit form for the susceptibility as a functional of the (self-consistently determined) paramagnetic self-energy. Since the expressions are rather long, we do not give them here.

2. Optical conductivity

The optical conductivity in linear response is given by the retarded current-polarization GF[38]:

$$\sigma^{\beta\alpha}(E) = -\langle\langle \hat{j}^\beta; \hat{P}^\alpha\rangle\rangle_E, \tag{11}$$

where α, β denote the Cartesian coordinates of the operators. By writing down the EQM of this GF and exploiting the connection $\hat{\mathbf{j}} = -i\frac{1}{N}[\hat{\mathbf{P}}, H]_-$ this can be rewritten as

$$\sigma^{\beta\alpha}(E) = -\frac{\langle[\hat{j}^\beta, \hat{P}^\alpha]_-\rangle}{E} + iN\frac{\langle\langle \hat{j}^\beta; \hat{j}^\alpha\rangle\rangle}{E}. \tag{12}$$

For a tight binding (nearest-neighbor hopping) model the operators are given as $\hat{\mathbf{P}} = q\sum_{i,\sigma}\mathbf{R}_i\hat{n}_{i\sigma}$ and $\hat{\mathbf{j}} = -\frac{iq}{N}t\sum_{\langle im\rangle,\sigma}(\mathbf{R}_i - \mathbf{R}_m)c_{i\sigma}^+ c_{m\sigma}$. With these operators the first term of (12) can be calculated and in case of a simple cubic lattice simplified to give the zero frequency Drude weight of conductivity:

$$\mathrm{Re}\left[\sigma_D^{\beta\alpha}(E + i0^+)\right] = -\pi\delta_{\alpha\beta}\delta(E)\frac{2tq^2}{N}\sum_{\mathbf{k}\sigma}\cos(k_\alpha)\langle\hat{n}_{\mathbf{k}\sigma}\rangle. \tag{13}$$

The second term in (12) is the current-current GF. It represents the influence of electronic correlations. We approximate this GF on the "one loop" level in a diagrammatic expansion. The explicit calculation is given in Appendix C and it is shown that the real part consists of two parts. One is proportional to $\delta(E)$ and cancels the Drude peak in case of a local self-energy exactly. The second term yields

$$\mathrm{Re}\left[\sigma_C^{\beta\alpha}(E + i0^+)\right] = \delta_{\alpha\beta}\frac{\pi q^2}{N}\sum_{\mathbf{k}\sigma}v_{\mathbf{k}\alpha}v_{\mathbf{k}\beta}\int dx\, S_{\mathbf{k}\sigma}(E+x) \times S_{\mathbf{k}\sigma}(x)\frac{f_-(x) - f_-(E+x)}{E}, \tag{14}$$

with $v_{\mathbf{k}\alpha} = \partial_{k_\alpha}\epsilon_{\mathbf{k}}$.

Note that this approximation becomes a rigorous result in infinite dimensions because the self-energy is a local quantity and all higher vertex corrections vanish in this case.[39]

We will only show results for the contribution from (14) hoping that the exact cancellation is retained in the **k**-dependent case approximately at least. The neglect of vertex corrections cannot be justified rigorously in case of a **k**-dependent self-energy because Ward identities may be violated. We show therefore only results for the 3D sc lattice, where the **k** dependence of the self-energy is not so pronounced (especially at the Fermi level) and refer the reader to the more specialized literature for a thorough discussion of this point.[40]

III. COMPUTATIONAL METHODS

The self-energy (8) is a functional of the chemical potential and different correlation functions. It has to be calculated self-consistently. To this end we need a fast way of calculating integrals of the form

$$\langle\cdots\rangle = \frac{1}{N}\sum_{\mathbf{k}}\int dE f_-(E)F_{\mathbf{k}}(E)S_{\mathbf{k}}(E), \tag{15}$$

where $f_-(E)$ is the Fermi function, $F_{\mathbf{k}}(E)$ is a polynomial of low order in E, and $S_{\mathbf{k}}(E)$ is the full SD. It is hopeless to perform the four-dimensional integral directly because the SD is a strongly peaked function. However one can replace the energy integration by a sum over the poles of $f_-(E)$ in the upper complex plane. The usual Matsubara form of the Laurent expansion of $f_-(E)$ is not suitable here because it converges very slowly with an increasing number of poles. Recently Ozaki[41] proposed a different pole expansion for the Fermi function which gives a good approximation for a large energy domain down to very low temperatures with only a few hundred poles. We use this expansion for a numerical very accurate determination of the energy integral. The remaining **k** integration over the irreducible wedge of the Brillouin zone can then be performed directly.

For the exposed procedure we need the values of the SOPT self-energy at the Ozaki poles in the complex plane. For their determination we first rewrite (3) as a sum over shells of symmetry equivalent points:

$$\Sigma^{(\mathrm{SOC})}_{\mathbf{k}\sigma}(E) = U^2 \sum_{s=0}^{N} G^{(s)}_{\mathbf{k}} \Sigma^{(s)}_{\sigma}(E), \tag{16}$$

where $G^{(s)}_{\mathbf{k}}$ denotes the $\mathbf{k}$-dependent shell factor given by the sum over the exponentials in (3) within one shell and $\Sigma^{(s)}_{\sigma}(E)$ the remaining energy-dependent part. The imaginary part of the latter is given by

$$\mathrm{Im}\Sigma^{(s)}_{\sigma}(E) = -\pi \int dx \int dy S^{(0)}_{s\sigma}(x) S^{(0)}_{s-\sigma}(y) S^{(0)}_{s-\sigma}(x+y-E) \times F(x,y,x+y-E), \tag{17}$$

where $F(x,y,z)$ denotes the product of Fermi functions in (3). This twofold convolution can be solved very efficiently by a fast Fourier transform. From this $\Sigma^{(s)}_{\sigma}(E)$ can be obtained in the complex plane via the spectral representation of Green's functions.[38] The free-shell density of states needed for the calculation have been computed and stored beforehand to very high precision. The number of shells necessary to get converged results depends strongly on the coordination number of the underlying lattice. After some tests we have used 201 shells for the 2D and 61 shells for the 3D lattice for all calculations in this work, which was sufficient to get mostly converged self-energies.

IV. RESULTS AND DISCUSSION

Our $\mathbf{k}$-dependent self-energy allows the description of homogeneous phases (paramagnetic/ferromagnetic). We will discuss the electronic properties in the paramagnetic state of the three-dimensional Hubbard model first, knowing well that in certain parameter regimes (e.g., near half-filling at low temperatures) antiferromagnetism is expected in principle. This restriction is shared with other self-energy approaches (e.g., DMFT calculations) and a comparison to these should render our results useful.

A. QDOS and spectral density

In Fig. 1 we show the quasiparticle density of states (QDOS) at low temperature ($T = 10$ K) for two different band fillings and various interaction parameters U. The three peak structure of the QDOS is clearly visible. Upper and lower Hubbard bands are roughly separated by the Coulomb interaction strength U and there appears a Kondo resonance near the Fermi level ($E = 0$ eV in figures). By increasing U, this resonance decreases but stays finite also for large U. As a consequence there is no clear metal-insulator transition (MIT) for $n = 1$ as is found in DMFT calculations. To illustrate this further we show the inverse effective mass $\frac{m}{m^*} = \frac{1}{N}\sum_{\mathbf{k}}[1 - \Re\Sigma'_{\mathbf{k}}(0)]^{-1}$ in Fig. 2. Although there is no clear transition point, the system should be insulating above $U/W \approx 10$ due to the large effective mass of the quasiparticles. This finding is in qualitative agreement with the nonlocal theory of Kakehashi and Fulde.[15]

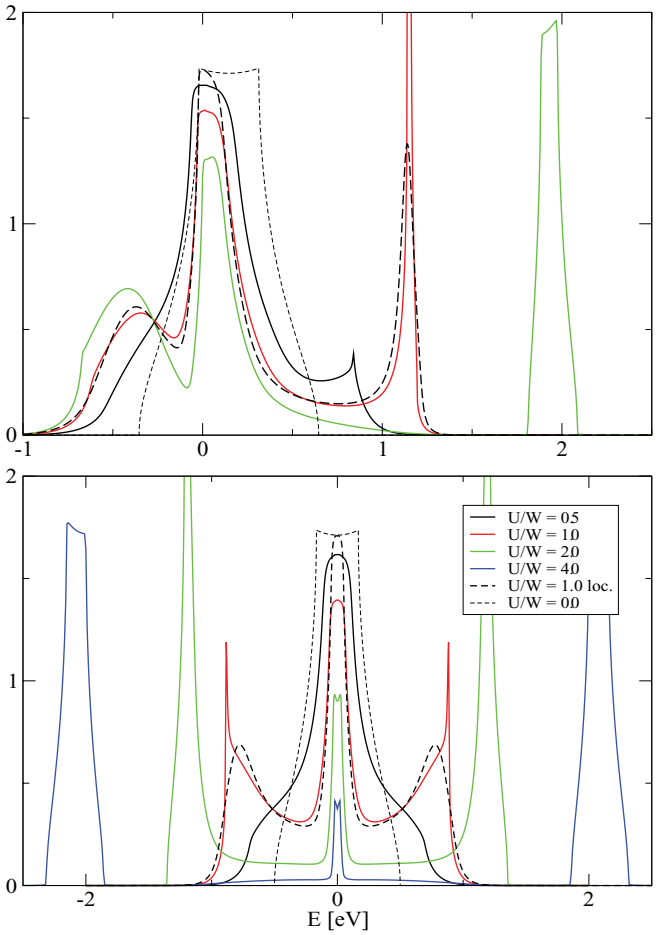

FIG. 1. (Color online) QDOS for various interaction parameters U/W; full lines: $\mathbf{k}$-dependent self-energy results; dashed lines: local self-energy and interaction free result. Parameters: $T = 10$ K, upper panel: $n = 0.75$, lower panel: $n = 1.0$.

The comparison of the local approximation (only the zeroth shell of the SOC is taken into account) and the full $\mathbf{k}$-dependent calculation shows decisive effects of the latter. Whereas the local theory fulfills the Luttinger theorem (the QDOS at the Fermi level is equal to the free DOS), the $\mathbf{k}$ dependence leads to a reduction of states at this point. This is understandable because the Luttinger-Ward argument only holds for local self-energies.[42,43] Another effect of the k dependence are the peaks in the upper ($n = 0.75, 1.0$) and lower ($n = 1.0$) Hubbard band for intermediate coupling ($U/W \approx 1$). For interpretation of these peaks we have plotted the spectral density together with the imaginary part of the self-energy along special directions within the first Brillouin zone for $n = 1$ in Fig. 3. The self-energy shows typical Fermi liquid behavior. The imaginary part is near zero (zero only at $T = 0$) at the Fermi level and decreases quadratically with increasing energy. This leads to increasing damping effects in the dispersion of the Kondo resonance particularly strong at the Γ and R points. At these points the self-energy shows a strong enhancement around $E = \pm 0.5$, respectively, and then increases abruptly to zero for lower/higher energies. Therefore we find no damping effects in this energy region and quasiparticle states with energies lower/higher than the threshold energy will have

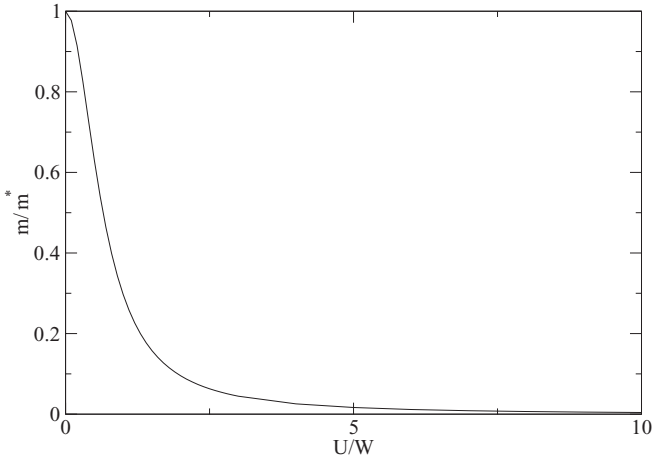

FIG. 2. Inverse effective mass as function of interaction parameter U/W. Parameters: $T = 10$ K, $n = 1.0$.

infinite lifetimes. This is clearly visible in the spectral density where in the lower/upper Hubbard band "bridges" of sharply peaked states appear at both **k** points. Similar effects were found in SOPT calculations by Schweitzer and Czycholl[14] and in the projection operator method of Kakehashi and Fulde[15] but here they are much more pronounced. The reason is most likely the increased numerical accuracy of our calculation (see Sec. III).

Comparing our results to a recent *dynamical cluster approximation*[13] (a cluster extension of the DMFT in order to retain a **k** dependence) there is good agreement below the MIT ($U/W = 0.67$ in the mentioned work). The dispersion of the Kondo resonance and the maxima of the lower/upper Hubbard bands show essentially the same behavior as in our calculation. Above the MIT ($U/W = 1$) there are of course discrepancies because of the missing MIT in the MPT.

With increasing temperature damping effects will become more important. This is shown in Fig. 4. The Kondo resonance peak is diminished with rising temperature and tend to vanish

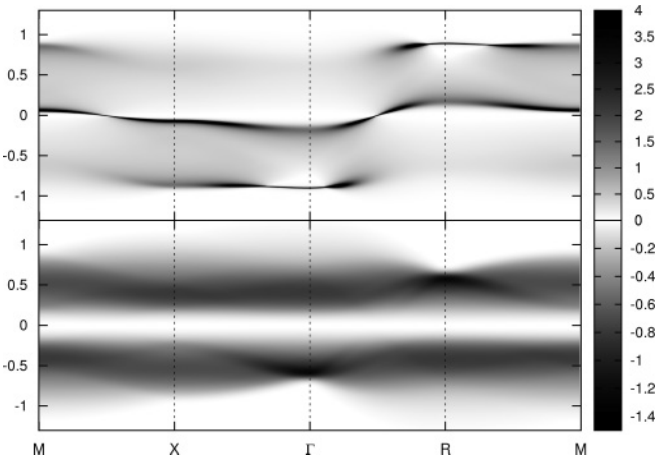

FIG. 3. Spectral density (upper figure) and imaginary part of MPT self-energy (lower figure) along special directions in the first Brillouin zone of the simple cubic 3D lattice: $M(\pi,\pi,0) \rightarrow X(\pi,0,0) \rightarrow \Gamma(0,0,0) \rightarrow R(\pi,\pi,\pi) \rightarrow M$. Parameters: $n = 1$, $T = 10$ K, $U/W = 1$.

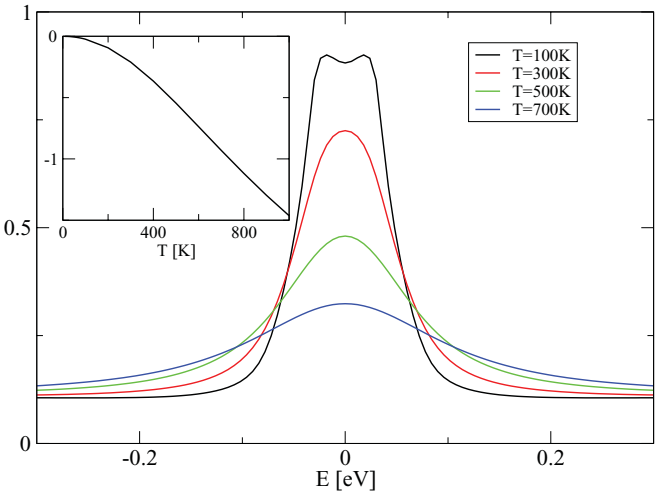

FIG. 4. (Color online) QDOS (Kondo resonance) at various temperatures T. Inset: averaged imaginary part of MPT self-energy at Fermi level $E = 0$. Parameters: $n = 1$, $U/W = 2$.

completely at higher temperatures. The reason for this can be found in the inset of Fig. 4. With increasing temperature the averaged imaginary part of the self-energy at the Fermi level decreases starting from zero at $T = 0$ K. For low temperatures a typical Fermi liquid behavior is obtained ($\sim T^2$).

For the two-dimensional sc lattice the effects of a nonlocal self-energy should be more drastic then in 3D as a direct consequence of the reduced coordination number. Figure 5 shows the spectral density and imaginary part of the self-energy of the sc 2D lattice at half-filling. We find again states with infinite lifetime at Γ and M points due to the vanishing imaginary part of the self-energy. The self-energy shows Fermi liquid behavior ($\sim E^2$) at large portions of the Brillouin zone. However, this behavior is changed near the Fermi surface. At the X point and the midpoint between Γ and M $(\frac{\pi}{2},\frac{\pi}{2})$ the self-energy shows a linear energy dependence. This "marginal Fermi liquid" behavior is a direct consequence of the perfect nesting properties $[\epsilon(\mathbf{k}) \approx \epsilon(\mathbf{k}+\mathbf{Q})$, where $\mathbf{Q}$

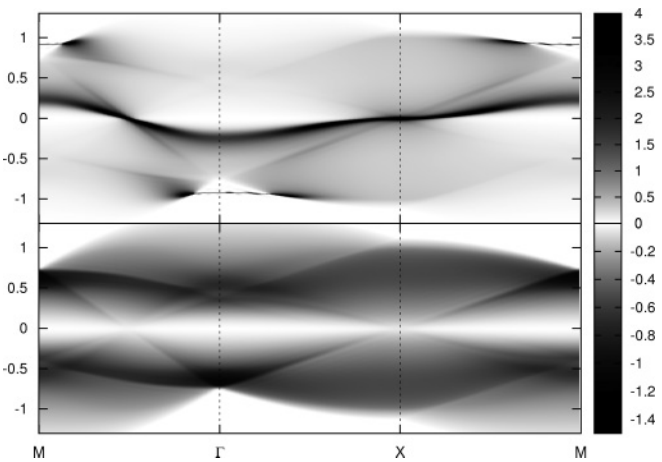

FIG. 5. Spectral density (upper figure) and imaginary part of MPT self-energy (lower figure) along special directions in the first Brillouin zone of the simple cubic 2D lattice: $M(\pi,\pi) \rightarrow \Gamma(0,0) \rightarrow X(\pi,0) \rightarrow M$. Parameters: $n = 1$, $T = 10$ K, $U/W = 1$.

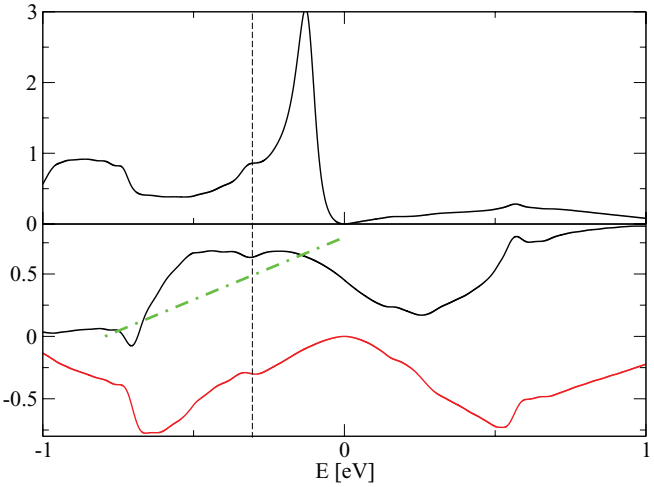

FIG. 6. (Color online) Spectral density (upper figure) and real part (lower figure: black line) and imaginary part (red line) of the self-energy for the simple cubic 2D lattice at $\mathbf{k} = (\frac{6\pi}{20}, \frac{6\pi}{20})$. Vertical broken line: position of the shadow band. The crossing point the green dash-dotted line with the real part of the self-energy marks the position of quasiparticle excitations. Parameters: $n = 1$, $U/W = 1$, $T = 10$ K.

is a reciprocal lattice vector] of the 2D Fermi surface[44,45] at half-filling. Electrons can be scattered efficiently due to the large phase space. This leads to a second effect in the spectral density—the formation of "shadow" bands. They are visible as dark lines running from the special points X, $(\frac{\pi}{2}, \frac{\pi}{2})$ to Γ, M with a slope determined by the condition $E \approx \epsilon(\mathbf{k} + \mathbf{Q})$. These shadow features, which have already been described by Vilk,[46] are no real quasiparticle band but merely thermal excitations corresponding to a local minimum of the imaginary part of the self-energy. To illustrate this point we have plotted the spectral density (upper panel) and self-energy (lower panel) at $\mathbf{k} = (\frac{6\pi}{20}, \frac{6\pi}{20})$ in Fig. 6. The green dash-dotted line obeys $E + \mu - \epsilon(\mathbf{k})$ and its crossing points with the real part of the SE (black line) define the quasiparticle excitations of the system. In the SD only one of the three excitations forms a peak (near $E = 0$), the others are strongly damped by a large imaginary part of the SE (red line). The black dashed line marks the position of the shadow band. There is no real excitation energy but we find a local minimum of the imaginary part of the SE which leads to observed shadow feature.

B. Conductivity

From (14) it becomes clear that the optical conductivity is mainly determined by the number of available quasiparticle states. In Fig. 7 the inverse static conductivity (resistivity) at half-filling is shown as a function of temperature for $U = 2$. At low temperatures the resistivity increases quadratically. This results from the reduction of the QDOS at Fermi level as shown in Fig. 4. The resistivity rises until the thermal energy is sufficient to excite electrons from the lower to the upper Hubbard band ($k_B T \approx U$). Then it will decrease going through a minimum and rise again. The inset shows the optical conductivity at fixed temperature $T = 100$ K. The conductivity decreases with increasing energy due to the lack of states between the Kondo resonance and the

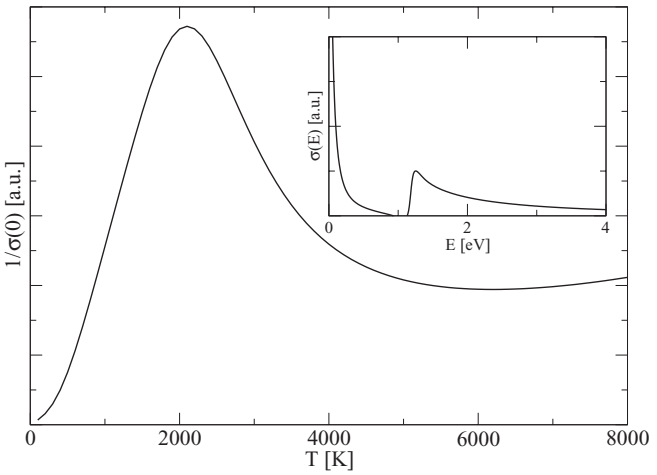

FIG. 7. Correlation part of the resistivity (inverse of the static conductivity) as a function of temperature T for the 3D simple cubic lattice. Inset: optical conductivity as function of E. Parameters: $n = 1$, $U = 2$. Inset: $T = 100$ K.

upper Hubbard band. As soon as the energy is sufficient to excite electrons from the Fermi level to the upper band, the conductivity will rise strongly reaching a maximum soon and decrease again. These findings for the conductivity are in good agreement with DMFT results for U below the metal-insulator transition.[39]

C. Inverse paramagnetic susceptibility and ferromagnetic phase transition

The inverse paramagnetic static susceptibility (IPS) (10) can be used as a tool for finding borders of a ferromagnetic phase transition in the n-U diagram. Its zero crossings will mark the critical points. In Fig. 8 we show the IPS for the 2D and 3D sc lattice at low temperature ($T = 10$ K) for various U. Whereas we find zero crossings above a critical $U/W \approx 15$ in the 3D case, there is no point of phase transition in the 2D

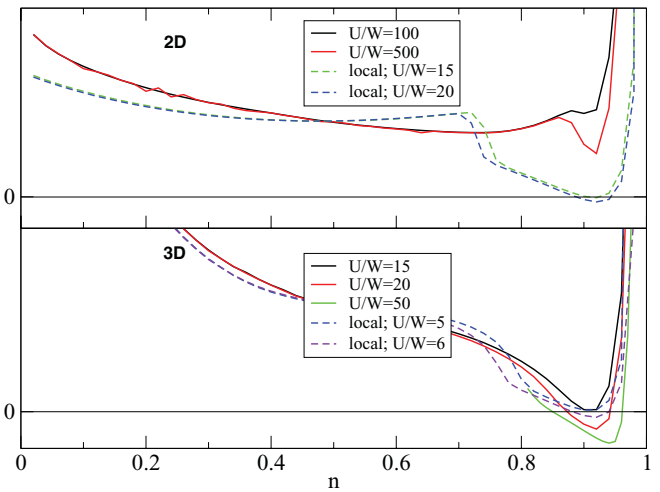

FIG. 8. (Color online) Inverse paramagnetic susceptibility as a function of band filling n for the 2D (upper figure) and 3D (lower figure) system calculated with the full $\mathbf{k}$-dependent self-energy. The result of local self-energy is shown also (dashed lines). Parameters: $T = 10$ K.

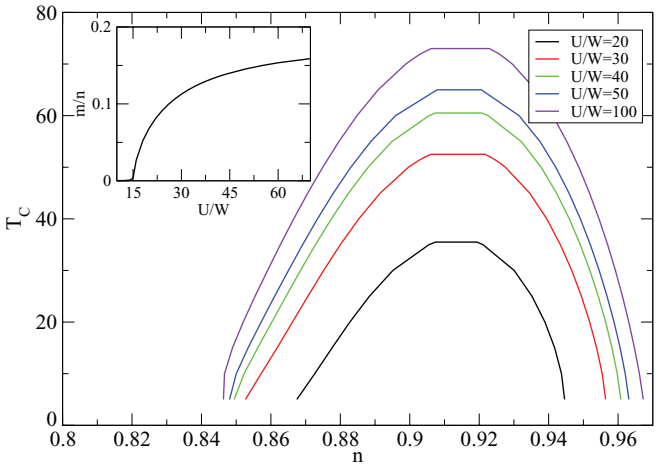

FIG. 9. (Color online) Curie temperature T_C as function of band filling n for various U/W. Inset: relative magnetization $(n_\uparrow - n_\downarrow)/n$ as function of interaction strength U/W. Parameters inset: $n = 0.9$, $T = 10$ K.

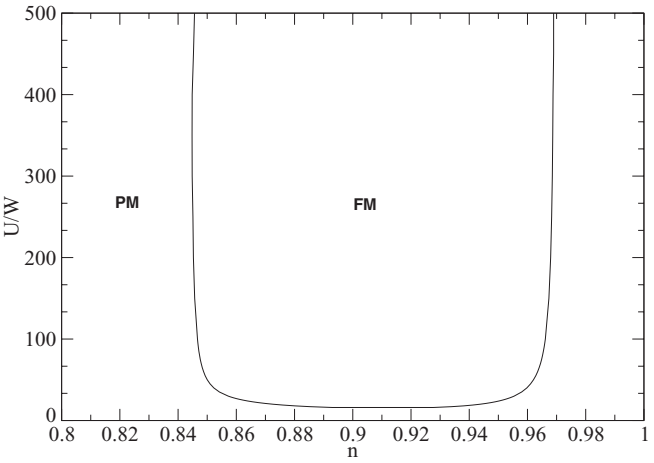

FIG. 10. Ferromagnetic phase diagram of the 3D simple cubic lattice as function of U/W and band filling n. Parameters: $T = 10$ K.

case when we use the full nonlocal MPT self-energy. Only when using the truncated local version of the MPT do we get a phase transition in 2D also. This shows first of all that the predictions of the nonlocal theory are in accordance with the Mermin-Wagner theorem and secondly, that the nonlocality of the self-energy is crucial in order to get the result. We would like to mention that the IPS curve for $U/W = 500$ is saturated in the sense that increasing U/W further will not change its shape drastically.

We come now to the discussion of the magnetic properties of the 3D system. The rather high critical U reflects the fact that the sc lattice is not particularly susceptible to ferromagnetism (the competing antiferromagnetism is not suppressed by frustration, like in the fcc lattice). The IPS crosses the zero axis at two points. These mark the lower and upper bound of the ferromagnetic region. The Curie temperatures for different U/W are plotted in Fig. 9. The maximal T_C is reached for a band filling of $n \approx 0.91$. Starting from $U_{\text{crit}}/W \approx 15$, T_C increases quickly with increasing U/W and runs into saturation for larger values of U/W. The same is true for the magnetization $m = n_\uparrow - n_\downarrow$ and the phase border. The magnetization at $n = 0.9$ and $T = 10$ K is shown in the inset of Fig. 9. The electron system is far from saturation, the polarization reaches $\sim$16% for $U/W = 70$ and increases slowly for stronger interaction parameters.

The full phase diagram is shown in Fig. 10. The lower phase boundary is decreasing with increasing U/W to lower n up to $U/W \sim 350$ where it takes the value $n_{\text{crit}} \approx 0.845$. Increasing U/W further will not increase the ferromagnetic region but we observe a slight shifting to higher n again. The upper phase boundary growths monotonically with increasing U/W reaching a value of $n \approx 0.969$ for $U/W = 500$. This result is in accordance with Nagaokas theorem.

As expected, in the local approximation the critical U: $U_{\text{crit}}/W \approx 5$ at $T = 10$ K for the 3D sc lattice is lower than in the full **k**-dependent case and agrees well with findings from DMFT calculations ($U/W \gtrsim 3$).[25]

V. SUMMARY AND CONCLUSIONS

In this work we have derived a nonlocal self-energy for the Hubbard model within a modified perturbation theory approach. It was shown that this self-energy fulfills a variety of limiting cases (e.g., weak coupling and atomic limit) and shows the correct high-energy behavior by construction. Numerical tools for the evaluation of this self-energy were introduced, in particular to solve the complicated momentum integrations.

We show results for the two- and three-dimensional simple cubic lattice, discussing in detail the influence of nonlocality, temperature, and interaction strength on the self-energy, spectral density, and quasiparticle density of states. These results are then used for the interpretation of the calculated optical conductivity and resistivity curves.

The inverse paramagnetic susceptibility was calculated, showing that there is no ferromagnetic phase transition in the two-dimensional but for the three-dimensional lattice. The ferromagnetic/paramagnetic phase diagram for the three-dimensional lattice is then constructed.

Our findings emphasize the importance of nonlocal correlations in the Hubbard model in low dimensions, in particular for the fulfillment of Mermin-Wagner theorem.

The strength of the present approach is that it allows self-consistent calculations at arbitrary band fillings with a fully **k**-dependent self-energy. This comes at the expense of neglecting certain correlation effects. Most severe in this respect is the missing metal-insulator transition (MIT) at half-filling, which should also occur in finite dimensions at roughly $U/W \approx 1$ as indicated by DMFT calculations.[13] It is interesting to note that the (local) MPT, when used as an impurity solver in a DMFT calculation for the infinite dimensional Hubbard model, does show a MIT in the correct U/W region, whereas it does not when used as a self-energy for the lattice Hamiltonian.[47]

Another shortcoming of the current state of the theory is the inability to check for antiferromagnetic phases, which ultimately should appear near half-filling. The reason for this is in the ansatz of the self-energy (8), which only allows the calculation of homogeneous phases. This does not mean that there are no possible antiferromagnetic solutions within the MPT approach. It would be an interesting task for a

forthcoming work to extend the MPT in this direction. An indirect hint for the presence of antiferromagnetic correlations within the MPT can be derived from the breakdown of ferromagnetic order near half-filling, which could have its origin in competing antiferromagnetic correlations.

APPENDIX A: COEFFICIENTS OF SELF-ENERGY EXPANSION

$$\begin{aligned} C^{(0)}_{\mathbf{k}\sigma} &= U\langle n_{-\sigma}\rangle, \\ C^{(1)}_{\mathbf{k}\sigma} &= U^2\langle n_{-\sigma}\rangle(1-\langle n_{-\sigma}\rangle), \\ C^{(2)}_{\mathbf{k}\sigma} &= C^{(1)}_{\mathbf{k}\sigma}\left[\epsilon_\sigma(\mathbf{k})-\mu+U(1-\langle n_{-\sigma}\rangle)\right]+U^2B_{\mathbf{k}-\sigma} \end{aligned} \tag{A1}$$

with

$$\begin{aligned} B_{\mathbf{k}-\sigma} &= B_{S,-\sigma}+B_{W,-\sigma}(\mathbf{k}), \\ B_{S,-\sigma} &= \frac{1}{N}\sum_{i,j}^{i\neq j}T_{ij}\langle c^+_{i-\sigma}c_{j-\sigma}(2n_{i\sigma}-1)\rangle \\ &= \frac{1}{N}\sum_{\mathbf{k}}[\epsilon(\mathbf{k})-T_0]\int_{-\infty}^{\infty}dEf_-(E) \\ &\quad\times\left\{\frac{2}{U}[E-\epsilon_{-\sigma}(\mathbf{k})]-1\right\}S_{\mathbf{k}-\sigma}(E-\mu), \\ B_{W,-\sigma}(\mathbf{k}) &= \frac{1}{N}\sum_{i,j}^{i\neq j}T_{ij}e^{-i\mathbf{k}(\mathbf{R}_i-\mathbf{R}_j)}(\langle n_{i-\sigma}n_{j-\sigma}\rangle-\langle n_{-\sigma}\rangle \\ &\quad-\langle c^+_{j\sigma}c^+_{j-\sigma}c_{i-\sigma}c_{i\sigma}\rangle-\langle c^+_{j\sigma}c^+_{i-\sigma}c_{j-\sigma}c_{i\sigma}\rangle). \end{aligned} \tag{A2}$$

APPENDIX B: HIGH ENERGY EXPANSION OF SOPT SELF-ENERGY

$$\Sigma^{(\mathrm{SOC})}_{\mathbf{k}\sigma}(E)\approx\sum_{m=1}^{N}\frac{D^{(m)}_{\mathbf{k}\sigma}}{E^m} \tag{B1}$$

with

$$\begin{aligned} D^{(1)}_{\mathbf{k}\sigma} &= U^2\langle n_{-\sigma}\rangle(1-\langle n_{-\sigma}\rangle)=C^{(1)}_{\mathbf{k}\sigma}, \\ D^{(2)}_{\mathbf{k}\sigma} &= U^2\sum_{\mathbf{R}}e^{i\mathbf{k}\mathbf{R}}\{\delta_{\mathbf{R},\mathbf{0}}[\langle e_{\mathbf{R}-\sigma}\rangle^{(0)}(2\langle n_{\mathbf{R}\sigma}\rangle^{(0)}-1) \\ &\quad+\langle n_{\mathbf{R}-\sigma}\rangle^{(0)}(M_{\mathbf{R}-\sigma}+M_{\mathbf{R}\sigma})]-\langle n_{\mathbf{R}-\sigma}\rangle(2M_{\mathbf{R}-\sigma}\langle n_{\mathbf{R}\sigma}\rangle^{(0)} \\ &\quad+M_{\mathbf{R}\sigma}\langle n_{\mathbf{R}-\sigma}\rangle^{(0)})\} \end{aligned} \tag{B2}$$

and

$$\langle n_{\mathbf{R}\sigma}\rangle^{(0)}=\int dEf_-(E)S^{(0)}_{\mathbf{R}\sigma}(E), \tag{B3}$$

$$\langle e_{\mathbf{R}\sigma}\rangle^{(0)}=\int dEEf_-(E)S^{(0)}_{\mathbf{R}\sigma}(E), \tag{B4}$$

$$M_{\mathbf{R}\sigma}=T_{\mathbf{R}}-\mu^{(0)}_{\sigma}\delta_{\mathbf{R},\mathbf{0}}. \tag{B5}$$

APPENDIX C: DERIVATION OF THE OPTICAL CONDUCTIVITY

The density-density GF in (renomalized: free propagators are replaced by full ones) diagrammatic one-loop expansion is given by

$$\begin{aligned} \langle\langle\hat{n}_{\mathbf{k}\sigma};\hat{n}_{\mathbf{k}'\sigma}\rangle\rangle_{E_n} &\approx \delta_{\mathbf{k}\mathbf{k}'}\frac{1}{\beta}\sum_m G_{\mathbf{k}\sigma}(iE_m)G_{\mathbf{k}\sigma}(iE_n+iE_m) \\ &= \delta_{\mathbf{k}\mathbf{k}'}\int\int dxdyS_{\mathbf{k}\sigma}(x)S_{\mathbf{k}\sigma}(y)\frac{f_-(x)-f_-(y)}{iE_n+x-y} \\ &\overset{(iE_n\to E+i0^+)}{=} \delta_{\mathbf{k}\mathbf{k}'}\int dxf_-(x)S_{\mathbf{k}\sigma}(x)[G_{\mathbf{k}\sigma}(x+E+i0^+)+G_{\mathbf{k}\sigma}(x-E-i0^+)]. \end{aligned}$$

From this we get for the correlation part of conductivity (12):

$$\begin{aligned} \mathrm{Re}\sigma^{\beta\alpha}_{II}(E+i0^+) &= \mathrm{Re}\left\{\frac{iq^2}{(E+i0^+)}\frac{1}{N}\sum_{\mathbf{k}\sigma}(\partial_{k_\beta}\epsilon_{\mathbf{k}})(\partial_{k_\alpha}\epsilon_{\mathbf{k}})\int dxf_-(x)S_{\mathbf{k}\sigma}(x)[G_{\mathbf{k}\sigma}(x+E+i0^+)+G_{\mathbf{k}\sigma}(x-E-i0^+)]\right\} \\ &= -2q^2\delta(E)\frac{1}{N}\sum_{\mathbf{k}\sigma}(\partial_{k_\beta}\epsilon_{\mathbf{k}})(\partial_{k_\alpha}\epsilon_{\mathbf{k}})\int dxf_-(x)\,[\mathrm{Im}G_{\mathbf{k}\sigma}(x)\mathrm{Re}G_{\mathbf{k}\sigma}(x)] \\ &\quad+\frac{\pi q^2}{E}\frac{1}{N}\sum_{\mathbf{k}\sigma}(\partial_{k_\beta}\epsilon_{\mathbf{k}})(\partial_{k_\alpha}\epsilon_{\mathbf{k}})\int dxf_-(x)S_{\mathbf{k}\sigma}(x)\,[S_{\mathbf{k}\sigma}(x+E)-S_{\mathbf{k}\sigma}(x-E)]\,. \end{aligned}$$

The first term of this result can be recast into the form of the Drude contribution (13) but with opposite sign:

$$\begin{aligned} -2q^2\delta(E)\frac{1}{N}\sum_{\mathbf{k}\sigma}(\partial_{k_\beta}\epsilon_{\mathbf{k}})(\partial_{k_\alpha}\epsilon_{\mathbf{k}})\int dxf_-(x)\,[\mathrm{Im}G_{\mathbf{k}\sigma}(x)\mathrm{Re}G_{\mathbf{k}\sigma}(x)] &= -q^2\delta(E)\frac{1}{N}\sum_{\mathbf{k}\sigma}(\partial_{k_\beta}\epsilon_{\mathbf{k}})(\partial_{k_\alpha}\epsilon_{\mathbf{k}})\int dxf_-(x)\mathrm{Im}\,[G_{\mathbf{k}\sigma}(x)]^2 \\ &= -q^2\delta(E)\frac{1}{N}\sum_{\mathbf{k}\sigma}(\partial_{k_\beta}\epsilon_{\mathbf{k}})(\partial_{k_\alpha}\epsilon_{\mathbf{k}})\int dxf_-(x)\frac{1}{\partial_{k_\alpha}\epsilon_{\mathbf{k}}}\partial_{k_\alpha}\mathrm{Im}G_{\mathbf{k}\sigma}(x) \end{aligned}$$

$$= -\pi q^2 \delta(E) \frac{1}{N} \sum_{\mathbf{k}\sigma} (\partial_{k_\alpha} \partial_{k_\beta} \epsilon_{\mathbf{k}}) \int dx f_-(x) S_{\mathbf{k}\sigma}(x) = -\delta_{\alpha\beta} \pi \delta(E) q^2 \frac{1}{N} \sum_{\mathbf{k}\sigma} (\partial_{k_\alpha}^2 \epsilon_{\mathbf{k}}) \langle \hat{n}_{\mathbf{k}\sigma} \rangle,$$

where the second and third step is only allowed when the self-energy does not depend on **k** and several steps require a diagonal mass tensor (as it is for the sc lattice).

*henning@physik.hu-berlin.de

[1] H. Capellmann, *Metallic Magnetism* (Springer, Berlin, 1987).
[2] J. Hubbard, Proc. R. Soc. London Ser. A **276**, 238 (1963).
[3] J. Kanamori, Prog. Theor. Phys. **30**, 275 (1963).
[4] M. C. Gutzwiller, Phys. Rev. Lett. **10**, 159 (1963).
[5] W. Metzner and D. Vollhardt, Phys. Rev. Lett. **62**, 324 (1989).
[6] E. Müller-Hartmann, Z. Phys. B **74**, 507 (1989).
[7] A. Georges, G. Kotliar, W. Krauth, and M. J. Rozenberg, Rev. Mod. Phys. **68**, 13 (1996).
[8] E. Gull, A. J. Millis, A. I. Lichtenstein, A. N. Rubtsov, M. Troyer, and P. Werner, Rev. Mod. Phys. **83**, 349 (2011).
[9] T. Maier, M. Jarrell, T. Pruschke, and M. H. Hettler, Rev. Mod. Phys. **77**, 1027 (2005).
[10] A. Toschi, A. A. Katanin, and K. Held, Phys. Rev. B **75**, 045118 (2007).
[11] M. V. Sadovskii, I. A. Nekrasov, E. Z. Kuchinskii, T. Pruschke, and V. I. Anisimov, Phys. Rev. B **72**, 155105 (2005).
[12] A. N. Rubtsov, M. I. Katsnelson, and A. I. Lichtenstein, Phys. Rev. B **77**, 033101 (2008).
[13] S. Fuchs, E. Gull, M. Troyer, M. Jarrell, and T. Pruschke, Phys. Rev. B **83**, 235113 (2011).
[14] H. Schweitzer and G. Czycholl, Z. Phys. B **83**, 93 (1991).
[15] Y. Kakehashi and P. Fulde, Phys. Rev. B **70**, 195102 (2004).
[16] Y. Nagaoka, Phys. Rev. **147**, 392 (1966).
[17] N. D. Mermin and H. Wagner, Phys. Rev. Lett. **17**, 1133 (1966).
[18] D. K. Ghosh, Phys. Rev. Lett. **27**, 1584 (1971).
[19] A. Gelfert and W. Nolting, Phys. Status Solidi B **217**, 805 (2000).
[20] W. Nolting and A. Ramakanth, *Quantum Theory of Magnetism* (Springer, Berlin, 2009).
[21] T. Obermeier, T. Pruschke, and J. Keller, Phys. Rev. B **56**, R8479 (1997).
[22] R. Zitzler, T. Pruschke, and R. Bulla, Eur. Phys. J. B **27**, 473 (2002).
[23] M. Ulmke, Eur. Phys. J. B **1**, 301 (1998).
[24] D. Vollhardt, N. Blümer, K. Held, M. Kollar, J. Schlipf, M. Ulmke, and J. Wahle, in *Advances in Solid State Physics*, edited by B. Kramer (Springer, Berlin, 1999), Vol. 68, pp. 383–396.
[25] S. Schmitt, N. Grewe, and T. Jabben, Phys. Rev. B **85**, 024404 (2012).
[26] R. Peters and T. Pruschke, New J. Phys. **11**, 083022 (2009).
[27] T. Herrmann and W. Nolting, J. Magn. Magn. Mater. **170**, 253 (1997).
[28] T. Herrmann and W. Nolting, Solid State Commun. **103**, 351 (1997).
[29] T. Hanisch, G. S. Uhrig, and E. Müller-Hartmann, Phys. Rev. B **56**, 13960 (1997).
[30] P. Fazekas, B. Menge, and E. Müller-Hartmann, Z. Phys. B **78**, 69 (1990).
[31] F. Günther, G. Seibold, and J. Lorenzana, Phys. Status Solidi B **248**, 339 (2011).
[32] This statement is not fully accurate since the first (Hartree) term contains a partial sum of diagrams of all orders already, when one chooses the full self-consistent $\langle n_{-\sigma} \rangle$ as we are doing in this work.
[33] D. Vollhardt, *Correlated Electron Systems* (World Scientific, Singapore, 1993).
[34] H. Kajueter and G. Kotliar, Phys. Rev. Lett. **77**, 131 (1996).
[35] M. Potthoff, T. Wegner, and W. Nolting, Phys. Rev. B **55**, 16132 (1997).
[36] A. B. Harris and R. V. Lange, Phys. Rev. **157**, 295 (1967).
[37] M. Potthoff, T. Herrmann, T. Wegner, and W. Nolting, Phys. Status Solidi B **210**, 199 (1998).
[38] W. Nolting, *Fundamentals of Many-Body Physics* (Springer, Berlin, 2009).
[39] T. Pruschke, D. L. Cox, and M. Jarrell, Phys. Rev. B **47**, 3553 (1993).
[40] D. Bergeron, V. Hankevych, B. Kyung, and A.-M. S. Tremblay, Phys. Rev. B **84**, 085128 (2011).
[41] T. Ozaki, Phys. Rev. B **75**, 035123 (2007).
[42] E. Müller-Hartmann, Z. Phys. B **76**, 211 (1989).
[43] J. M. Luttinger and J. C. Ward, Phys. Rev. **118**, 1417 (1960).
[44] J. E. Hirsch, Phys. Rev. B **31**, 4403 (1985).
[45] A. Virosztek and J. Ruvalds, Phys. Rev. B **42**, 4064 (1990).
[46] Y. M. Vilk, Phys. Rev. B **55**, 3870 (1997).
[47] K. Lichtner, Diploma thesis, Lehrstuhl für Theoretische Festkörperphysik, Humboldt Universität zu Berlin, 2009.